



HAL
open science

Enzymatic Glucose-Oxygen Biofuel Cells for Highly Efficient Interfacial Corrosion Protection

Aleksandar Karajić, Pascal Merzeau, Emmanuel Suraniti, Sébastien Gounel, Christèle Jaillet, Alexander Kuhn, Nicolas Mano

► **To cite this version:**

Aleksandar Karajić, Pascal Merzeau, Emmanuel Suraniti, Sébastien Gounel, Christèle Jaillet, et al.. Enzymatic Glucose-Oxygen Biofuel Cells for Highly Efficient Interfacial Corrosion Protection. ACS Applied Energy Materials, 2020, 3 (5), pp.4441-4448. 10.1021/acsaem.0c00140 . hal-02631799

HAL Id: hal-02631799

<https://hal.science/hal-02631799>

Submitted on 27 May 2020

HAL is a multi-disciplinary open access archive for the deposit and dissemination of scientific research documents, whether they are published or not. The documents may come from teaching and research institutions in France or abroad, or from public or private research centers.

L'archive ouverte pluridisciplinaire **HAL**, est destinée au dépôt et à la diffusion de documents scientifiques de niveau recherche, publiés ou non, émanant des établissements d'enseignement et de recherche français ou étrangers, des laboratoires publics ou privés.

Enzymatic glucose-oxygen biofuel cells for highly efficient interfacial corrosion protection

Aleksandar Karajic^{1,2}, Pascal Merzeau¹, Emmanuel Suraniti², Sébastien Gounel¹, Christèle Jaillet¹, Alexander Kuhn^{2}, Nicolas Mano^{1*}.*

¹ Centre de Recherche Paul Pascal (CRPP), CNRS UMR 5031, Univ. Bordeaux, 115 Avenue du Docteur Schweitzer, 33600 Pessac, France.

² Univ. Bordeaux, CNRS UMR 5255, Bordeaux INP, ENSCBP, 16 avenue Pey-Berland, 33600 Pessac, France.

Keywords: Glucose-oxygen biofuel cell, Corrosion protection, Bioelectronics, Boost converter, Bioelectrochemistry

ABSTRACT

Biofuel cells (BFCs) are electrochemical devices that rely on the transformation of chemical energy into electricity through biochemical pathways, however delivering only modest or low power and voltage. This intrinsic limitation narrows their potential applications for driving electronics and thermodynamic systems with higher energy demands than what can be delivered by the BFCs alone. Nevertheless, coupling BFCs to electronic circuits, able to raise their voltage, allows circumventing these drawbacks. In this proof-of-concept study, we demonstrate an unconventional way of achieving highly efficient electrochemical corrosion protection of an iron surface in a chloride rich medium. The required protecting cathodic potential is generated by a self-powered bioelectronic system, consisting of a BFC, which can, despite its low voltage

output (0.3V), completely prevent interfacial corrosion if it is combined with an electronic boost converter.

Introduction

Biofuel cells (BFC)¹⁻³ are low power electrochemical devices capable of transforming chemical into electrical energy either with immobilized enzymes³, microorganisms^{4,5} or living organelles⁶. Optimized over several decades by implementing new materials,⁷⁻⁹ fabrication technologies and strategies, BFCs nowadays are well-adapted to allow various practical applications, such as self-powered biosensors¹⁰⁻¹⁵, wearable electronics¹⁶ and “bio-batteries” for powering small electronic devices¹⁶⁻¹⁸. In enzymatic biofuel cells, those that rely on the biocatalytic oxidation of glucose and reduction of oxygen are among the most abundant examples reported in the literature due to the fact that glucose and oxygen are readily available in living organisms and can be easily replenished in biological fluids¹⁹.

The main drawbacks of biofuel cells are their low power/voltage output and limited lifetime, rendering them less suitable for continuous powering of small electronic devices than other energy storage/supply systems such as batteries. Many strategies have been explored in the past to boost the power output to the levels required for electronic circuits. This includes the implementation of different materials with high electrochemical active surface area (nano-²⁰ and macroporous²¹ materials, carbon-nanotubes²²⁻²⁴, graphene²⁵, etc.), the design of new enzyme mutants²⁶ with improved activity and stability or the use of boost converters able to enhance the output voltage generated by a BFC^{17,27}. However, the latter is only possible at the expense of the globally available power^{17,28} (i.e. biofuel-cell output), partially consumed by the boost converter for its proper functioning.

Few examples of biofuel cells connected to a boost converter for powering electronic devices/components such as pacemakers²⁹, electronic watches¹⁶, digital thermometers¹⁸, light emitting diodes^{18,30} or capacitors³¹, were reported in the literature. Recently, our group has demonstrated the concept of temporarily storing the energy released in one system (i.e. glucose/oxygen biofuel cell) in the form of electromagnetic energy, to drive another electrochemical reaction (i.e. water splitting) with an overall positive ΔG value ($\Delta G_{\text{glucose/oxygen}} < \Delta G_{\text{water splitting}}$), while sharing the same electrolyte. The system did not require any external power source and the circuit was composed of the BFC and a water electrolyzer, connected *via* a boost converter for the voltage increase and a flyback for galvanic separation.²⁸

In this proof-of-concept study, we examine the electrochemical corrosion protection of an iron surface in chloride containing PBS buffer by using an initially low voltage (0.3 V) generated by a single glucose/oxygen biofuel cell. The voltage generated in the BFC was modulated *via* a boost converter to reach a much higher value of 2.3 V, the minimum voltage level that is required for successful corrosion protection. To the best of our knowledge, this is the first study reporting total corrosion protection based on a simple glucose-oxygen BFC. These findings might open up new application opportunities for BFCs, far beyond the traditional areas of energy storage and conversion.

Experimental section

Materials

All aqueous solutions used in this work were prepared in MilliQ® water (18 MΩ cm) from analytical grade chemicals. D-glucose (99.6%), sulfuric acid (96%), sodium chloride ($\geq 99.5\%$), sodium hydrogen phosphate heptahydrate ($\geq 98\%$), sodium-dihydrogen phosphate monohydrate ($\geq 98\%$) and catalase (from bovine liver; activity: 14000 U mg⁻¹ of protein) were purchased from Sigma Aldrich. Iron rods (purity: 99+ %, Ø: 2 mm) were obtained from AlfaAesar. Agarose (electrophoresis grade) was obtained from Invitrogen™. Electrode polishing alumina slurry (0.05 μm) was purchased from Buehler (IL, USA). Glucose oxidase from *Aspergillus Niger* (activity: 480 U.mg⁻¹) was purchased from Sigma Aldrich and purified according to a previously published procedure.³² Bilirubin oxidase (BOD) from *Magnaporthe Oryzae* (activity: 568 U.mg⁻¹) was produced and purified as previously reported.³³ Gold-coated glass slides were purchased from Kerdry, France. Carboxylated multiwall carbon nanotubes (MWCNT-COOH; 0.54 wt.% in MilliQ water)^{34,35}, as well as anodic³⁶ and cathodic³⁷ Os-redox polymers were synthesized as reported earlier.

The electrochemical measurements that include the cleaning of the gold electrodes, corrosion studies and the characterization of the BFC were performed with a CH Instruments bi-potentiostat (842B or 760C). Ag/AgCl (3M NaCl) reference electrodes were purchased from BASi while the platinum wire used as a counter electrode was obtained from AlfaAesar. Glassy carbon rotating disc electrodes were purchased from Pine Research Instrumentation. PDMS monomer and initiator were purchased from GE Bayer Silicones (Leverkusen, Germany).

Preparation of planar gold electrodes

The 2.25 cm² squared gold-coated glass slide electrodes were prepared by soldering the electric leads and selecting a geometric surface area of approximately 2.25 cm² ($\approx 1.5\text{cm} \times 1.5\text{cm}$) with a thin layer of a commercially available nail varnish. Once the nail-varnish was completely dried, the electrochemical cleaning of the electrode surface was performed by cyclic voltammetry in an argon-saturated 100 mM H₂SO₄ solution. 50 CVs at 100 mV s⁻¹ were performed between -0.2 V to +1.6 V *vs.* Ag/AgCl (3M NaCl) until a steady shape of consecutive voltammograms is obtained. Then, the electrodes were rinsed with MilliQ water, dried in an argon stream and immediately used for the preparation of the glucose/oxygen biofuel cell.

Electrode potentials are expressed *versus* a Ag/AgCl (3M NaCl) reference electrode (referred to as Ag/AgCl) if not stated otherwise.

Biofuel cell preparation

The anodic hydrogel was prepared by mixing 43.5 μl of anodic Os-redox polymer (PVP-Os[(1,1-dimethyl-2,2'-biimidazole)2-2-[6-methylpyrid-2yl] imidazole]^{2+/3+}; γ : 8.0 mg.ml⁻¹ in MilliQ water) with 43.3 μl of glucose oxidase solution (γ : 5.0 mg.ml⁻¹ in MilliQ water) and 30.9 μl of polyethyleneglycol diglycidyl ether (PEGDGE) as a cross-linker (γ : 2.0 mg.ml⁻¹ in MilliQ water), respectively. The wt% ratio of the GOx/Os-polymer/PEGDGE in the anodic hydrogel was 35/55/10. 106.2 μl of the so-obtained hydrogel were carefully spread over the entire surface of a freshly cleaned gold electrode and dried at 4 °C for 48h. The final hydrogel loading was 250 $\mu\text{g.cm}^{-2}$.

For the preparation of the cathodic composite hydrogel, 80.6 μl of the cathodic Os-redox polymer (PAA-PVI-[Os(4,4'-dichloro-2,2'-bipyridine)₂Cl]⁺²⁺; γ : 10 mg.mL⁻¹ in MilliQ water) was mixed with 38.6 μl of BOD, 84.2 μl of MWCNT-COOH suspension (w: 0.054 wt.% in MilliQ water) and 23.9 μl of PEGDGE cross-linker, respectively. 198.6 μl of this composite suspension were spread onto the surface of the Au electrode and dried at 4 °C for 48h. The obtained composite MWCNT-COOH/hydrogel loading was 416.7 $\mu\text{g.cm}^{-2}$. The ratio between the cathodic hydrogel and MWCNT-COOH was 60/40 while the wt% ratio of BOD/Os-polymer/PEGDGE was kept at 30/62.57/7.43.

The bioelectrodes were removed from the fridge at least 1h before the electrochemical characterization. The BFC was assembled prior to its use with the two electrodes facing each other while a 7 mm thick PDMS spacer was introduced between them. The entire assembly was wrapped with a few layers of adhesive tape to ensure the structural integrity of the BFC.

PDMS was synthesized by thermal curing of a 10 : 1 = monomer: initiator mixture at 95 °C for 2h.

Optimization of the composition of MWCNT-COOH/BOD/Os-redox polymer/PEGDGE hydrogel composite

Cyclic-voltammetry on a rotating glassy carbon (GC) disc electrode modified with the composite BOD hydrogel was performed to determine the optimal MWCNT-COOH loading for the preparation of the cathodic hydrogel. For that purpose, a glassy-carbon electrode (\emptyset : 5 mm) was intensively polished with alumina slurry and thoroughly rinsed with MilliQ water. The surface of the so-prepared electrode was modified by drop-casting MWCNT-COOH/BOD based hydrogel-composite that contains different amounts of CNTs (i.e. 20, 30, 40, 50, 60 wt%). The loading of

the BOD/Os-redox polymer/PEGDGE hydrogel was kept constant at $108 \mu\text{g}\cdot\text{cm}^{-2}$. The cyclic voltammograms (potential window: +0.6 V to -0.15 V) were recorded in an argon and oxygen saturated PBS solution (20 mM PB + 140 mM NaCl) at 5 mV s^{-1} , $37.5 \text{ }^\circ\text{C}$, and 500 rpm with a Pt wire and Ag/AgCl serving as counter and reference electrodes, respectively. The cathodic $4e^-$ oxygen reduction diffusion-limited current was measured at -0.15 V.

Electrochemical characterization of the BFC

The electrochemical characterization of bioelectrodes was performed in a standard three-electrode electrochemical set-up with the enzymatic-hydrogel modified cathode/anode, a coiled Pt wire and Ag/AgCl serving as working, counter and reference electrodes, respectively. The platinum counter electrode was cleaned prior to every use in electrochemical experiments.

The size of a standard glass-body Ag/AgCl reference electrode was reduced by mounting a U-shaped glass capillary extension (i.e. made from a glass pipette) to its end. The opening of the extension was filled with 3M NaCl solution and sealed with a small agarose seal, serving as a salt bridge. For this purpose, a 2% agarose solution was prepared by dissolving agarose in 3M NaCl solution at $80 \text{ }^\circ\text{C}$. A small amount of the so-obtained solution was introduced by suction into the capillary end before the agarose gelified. The reference electrode was placed in the confined space between biocathode and bioanode during the electrochemical characterization experiments.

The electrochemical characterization of the separate bioelectrodes was performed by cyclic-voltammetry at 5 mV s^{-1} , $37.5 \text{ }^\circ\text{C}$ in phosphate buffer saline (PBS; 20 mM phosphate buffer + 140 mM NaCl; pH: 7.2) solution by cycling the potential between -0.3 V and +0.6 V. The first part of the electrochemical characterization was performed in an argon saturated PBS solution in

the absence of glucose and oxygen. This step is followed by the addition of a glucose stock solution (C_{final} : 50 mM), 20 nM catalase and intensive oxygen purging. The oxygen was purged through a space between two parallel electrodes for at least 10 minutes before the addition of glucose and catalase to ensure its saturation in PBS solution under experimental conditions.

The polarization curve was recorded at a scan rate of 5 mV s^{-1} in a two-electrode system with the bioanode connected to a potentiostat *via* short-circuited counter/reference electrode contacts and a biocathode that was connected as the working electrode. The BFC power curve was calculated by multiplying the current with the voltage measured during the polarization experiment.

Measurement of the MWCNT-COOH zeta potential

The Zeta potential of MWCNT-COOH suspended in MilliQ water was determined by using disposable cuvettes with a capillary channel and a Zetasizer Nano ZS apparatus (Malvern Instruments Ltd, Worcestershire, UK) in quintuplicate at $25 \text{ }^{\circ}\text{C}$.

Preparation of iron rods for the corrosion experiment

Iron rods were cut into 5 cm long pieces and the surface oxide layer was removed with sandpaper of different grit size (400, 800 and 1200, respectively) until a macroscopically smooth and polished surface was obtained. This step was followed by 5 min ultrasonication in absolute acetone and ethanol³⁸, respectively. Finally, the samples were dried in an argon stream and used for the corrosion experiment.

Optimization of the corrosion-preventing voltage

The influence of the applied voltage on the corrosion process in PBS solution was evaluated with a CH Instruments potentiostat/galvanostat (Model: 660C) in a two-electrode electrochemical cell composed of a Fe rod as working electrode and short-circuited counter-reference platinum electrodes. Different voltages were applied for 3h followed by extensive rinsing (i.e. MilliQ water and absolute ethanol, respectively) and drying (i.e. stream of argon) steps. Samples were preserved in an inert atmosphere until used.

Electrochemical impedance spectroscopy (EIS)

EIS measurements were performed on a CH Instruments potentiostat/galvanostat (Model: 660C) in PBS buffer (20 mM PB + 140 mM NaCl; pH: 7.2) with a three-electrode system composed of the Fe rod as working, a Pt coil as counter and Ag/AgCl as reference electrode. The EIS spectra were recorded around the OCV (i.e. 0.7 V; the OCV was measured continuously for 30 minutes), frequency range from 10^{-2} Hz to 10^5 Hz, and 10 mV amplitude.

The Fe rods used in EIS experiments were either in their pristine form (i.e. cleaned with sandpaper, acetone, and ethanol respectively) or after applying a corrosion-preventing voltage over a period of 4h. The control sample was immersed in PBS solution and left to corrode for 4h.

Scanning electron microscopy (SEM) characterization

SEM images were obtained by using a tabletop SEM microscope (TM-1000, Hitachi, Japan).

The EDS spectra were recorded with a field emission scanning electron microscope (JMS-6700F, JEOL Ltd., Japan).

Boost converter

A low-power BQ25505EVM-218 boost converter was purchased from Texas Instruments. To meet our specific requirements, the boost converter was modified with a 5 M Ω potentiometer in series with a 8.2 M Ω resistor, to make the output voltage tunable (**Figure S1, Supplementary Information**). The OCV was measured by the maximum power point tracker (MPPT) every 16 s in order to establish the voltage at which a maximum power is drained from the biofuel cell ($V_{P_{max}} \approx 45\%$ of the OCV). The current and the voltage at the input (output of the BFC) and the output (input of the corrosion cell) of the boost converter were continuously monitored by Keithley 2000 multimeters (Keithley, USA).

Results and Discussion

Optimization of the conditions for electrochemical corrosion protection

The first evaluation of the corrosion process was performed with an iron rod working electrode immersed in PBS combined with a short-circuited counter/reference Pt coil electrode. The values of the corrosion potential obtained from the potentiodynamic polarization experiment (**Figure S2**) show a higher thermodynamic instability of the Fe surface in PBS ($E_{corr.} = -1.16$ V vs. Pt) in comparison with NaCl solution ($E_{corr.} = -0.83$ V vs. Pt) commonly used in corrosion studies because of an intensive chloride-induced pitting corrosion.^{39,40} Another advantage of using PBS in this proof-of-concept study is the ability of phosphate ions to chemically capture the corrosion products (i.e. Fe²⁺ ions) in the form of a colored and insoluble phosphate/oxide heterogeneous layer that precipitates on the electrode surface. This has already been observed with either construction⁴¹ or carbon steel⁴² alloys. The EDS analysis of the corroded iron surface (**Figure S3**) confirmed the presence of a significant amount of surface oxygen and phosphorous atoms, originating from the iron oxide and phosphate.

The time-dependent evolution of the corrosion process is shown in **Figure S4**. The SEM images show that the corrosion process and the formation of the insoluble corrosion layer takes place soon after the substrate is immersed in PBS electrolyte (i.e. 3 min; **Figure S4a**). Further growth of the mixed oxide/phosphate corrosion crust occurs continuously with the formation of cracks that are present at its surface once a critical thickness is reached (**Figure S4e and f**). This indicates an extremely fast corrosion kinetics, expected for such a corrosion-prone, non-noble metal-based surface. The proposed mechanism for the corrosion of a pure iron surface in PBS buffer is shown in **Scheme S1**.

In order to optimize the voltage that needs to be applied in a Fe-Pt two-electrode system for successful electrochemical corrosion prevention, a series of chronoamperometric experiments were performed at different applied voltages. **Figure 1** depicts the SEM images of the samples subjected to voltages from -1.6 V to -2.3 V (vs. Pt reference) during 3h. SEM observation shows that voltages more negative than -2.2V are required for complete corrosion protection. The presence of microscopic grooves and surface imperfections, that can be observed on the high-magnification SEM images (e.g. **Fig. 1b and 1f**), originate from sharp SiC crystals present in the polishing paper and are not related to the corrosion process itself. EIS measurements were used for the further evaluation of the electrochemical corrosion protection concept. The obtained Nyquist plots (**Figure S5**) clearly show a significant increase in the charge-transfer resistance in the case of the control sample (no voltage applied; 4 h in PBS buffer) compared to the sample that was exposed to -2.3 V for 4 h. A small difference in the semicircle radius was observed between the pristine metal and a sample that was kept at -2.3 V. This can be ascribed to the presence of a thin iron-oxide layer that was spontaneously formed in the case of the pristine Fe

rod in comparison with the sample that was used immediately after the cleaning step for the corrosion protection and EIS experiments.

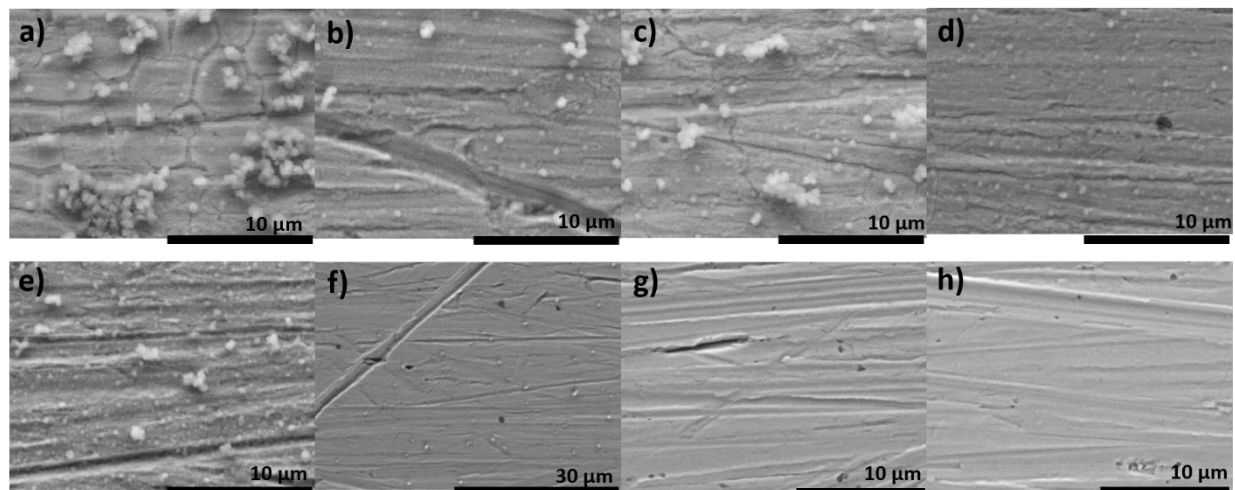


Figure 1. SEM images of iron samples that were exposed to different voltages: **a)** -1.6 V; **b)** -1.7 V; **c)** -1.8 V; **d)** -1.9 V; **e)** -2.0 V; **f)** -2.1 V; **g)** -2.2 V and to **h)** -2.3 V, respectively) in PBS electrolyte for 3h.

Biofuel cell engineering and characterization

Enzymatic bioelectrodes were prepared by modifying the selected (1.5 cm x 1.5 cm) area of gold-coated glass slides with the specially formulated enzymatic hydrogels consisting of cathodic bilirubin oxidase from *Magnaporthe Oryzae*³⁷, anodic glucose oxidase from *Aspergillus Niger*, a PEGDGE cross-linker and custom-designed cathodic and anodic Os-based redox polymers. They serve as redox mediators for an efficient wiring of the redox centers of the enzymes to the electrode surface, regardless of the orientation of the enzyme molecules within the hydrogel matrix.^{43,44}

The power generated by a BFC is often limited by the cathodic oxygen reduction reaction³⁷ due to its low solubility³ (i.e. 0.2 mM in water equilibrated with air at 37 °C)⁴⁵ and modest diffusion

coefficients⁴⁶ in aqueous media. To improve the power output of the biofuel cell by minimizing the above-mentioned cathodic limitations, MWCNT were incorporated into the cathodic hydrogel. The optimization of the ratio between BOD/Os-polymer/PEGDGE hydrogel and MWCNT-COOH was performed by cyclic voltammetry on glassy-carbon rotating disc electrodes in oxygen saturated PBS. The diffusion limited currents obtained at 37.5 °C and 500 rpm (**Figure S6**) show that the optimal ratio between BOD/Os-polymer/PEGDGE hydrogel and MWCNT-COOH is 60:40. Moreover, the low value of the measured zeta potential for MWCNT-COOH (ξ : -62.48 ± 2.92 mV; n: 5 measurements; 95% level of confidence) indicates the possibility for the formation of an electrostatic complex between the positively charged Os redox polymer molecules and the negatively charged deprotonated MWCNT-COOH. A similar mechanism of electrostatic interaction between the positively charged Os redox polymer and negatively charged enzyme molecules at physiological pH has been discussed in the literature.^{45,47} As a result, a better interaction is obtained between the MWCNT-COOH and the enzyme-containing hydrogel resulting in a better electron-transport throughout the volume of the composite hydrogel. In addition, the higher conductivity of MWCNT-COOH, along with a beneficial increase in active surface area allows to overcome the current limitations of the cathode.

The biofuel cell was constructed by placing the two electrodes in a parallel configuration relative to each other with a 7 mm thick PDMS spacer in between them (**Scheme S2**). Oxygen was supplied to the confined volume between the two electrodes through a pipette tip that was placed under the opening at the bottom of the biofuel cell. In that way, it ensured constant convection and delivery of the fresh amounts of glucose and oxygen.

Both the anode and cathode were first characterized separately under argon at a scan rate of 5 mV s⁻¹ (**Figure 2**). In the absence of substrates only two redox peaks (**Figure 2a**) corresponding to the reversible electrochemical oxidation/reduction of osmium redox centers can be observed at a formal potential of +0.30 V and -0.03 V, for the cathodic and anodic polymers, respectively. After addition of 50 mM glucose and O₂, characteristic sigmoidal voltammograms were obtained, corresponding to the reduction of oxygen at the cathode³⁷ (**black curve, Figure 2b**) and glucose oxidation at the anode (**blue curve, Figure 2b**). To extend the lifetime of the anode and the durability of the biofuel cell, 20 nM catalase was added to the PBS buffer to decompose hydrogen peroxide, a detrimental side product that may be formed at the anode when using osmium based redox polymers with redox potentials lower than + 0.07 V vs. Ag/AgCl (3M NaCl).⁴⁸

Polarization and power curves of the biofuel cell are present in the **Figure 2c**. The electrode potential was cycled between the open circuit voltage (OCV) (i.e. +0.75 V) and 0 V and the current was measured. The obtained results were used to plot the power curve that is the most important feature of biofuel cells. The maximum power was 500 μW at 0.3 V with a short-circuit current value of 2 mA. The obtained power was limited by the cathodic reaction, but it might be further improved by implementing gas-diffusion electrodes in order to overcome the relatively low oxygen solubility and mass transport constraints on the cathodic side.^{49,50}

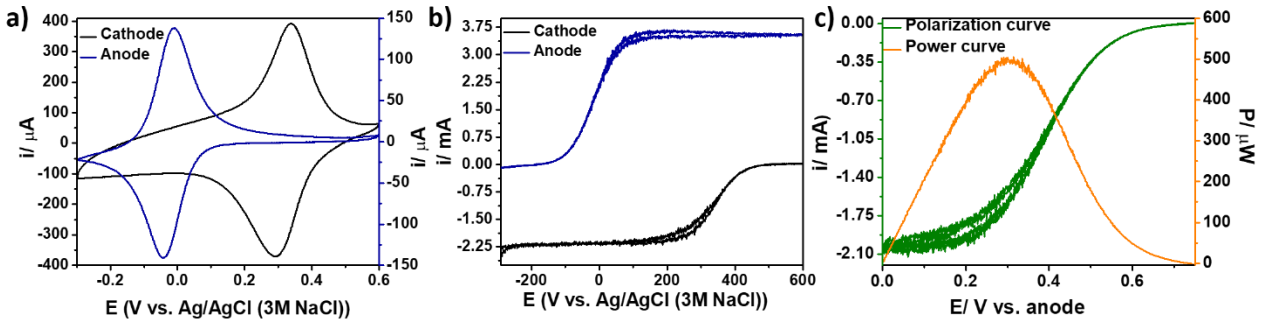


Figure 2. Cyclic voltammograms of BOD/Os-polymer/MWCNT-COOH/PEGDGE modified Au cathode (black curve) and GOx/Os-polymer/PEGDGE modified anode (blue curve) recorded at 5 mV s^{-1} , $37.5 \text{ }^\circ\text{C}$ in **a)** argon saturated PBS buffer in the absence of glucose and, **b)** in the presence 50 mM glucose in oxygen saturated PBS; **c)** Polarization (green) and power (orange) curves of the biofuel cell.

Bioelectronic interface for corrosion protection

The results of the optimization of the voltage needed between the iron rod serving as cathode and the coiled platinum anode show that a minimum of 2.2 V is necessary for the successful corrosion protection in PBS buffer. This voltage cannot be delivered by a single glucose-oxygen BFC which usually only can provide a maximum of 0.3 V under the present operating conditions. Therefore, a low-power boost converter (BC) was used to step-up the BFC voltage to the required value of 2.3 V that was supplied to the corrosion cell. The schematic set-up used in this study is shown in **Figure 3**.

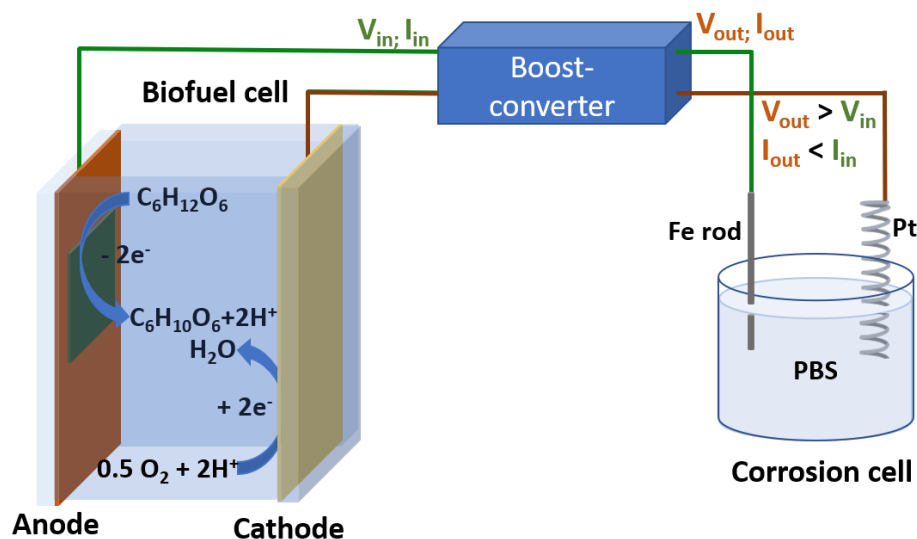


Figure 3. Schematic illustration of the bioelectronic-electrochemical system used in the corrosion protection study. The system consists of a biofuel cell, a boost converter and a corrosion cell.

The corrosion protection experiments were performed by connecting the BFC-BC interface endpoints to the Fe rod and the Pt wire immersed in PBS buffer. The input and the output voltage and the power curves of the BFC and the BC are shown in **Figure 4**. The boost converter could provide a stable voltage output of 2.3 V for 2 h until the voltage dropped to 2.2 V, a threshold value for successful corrosion protection (**Figure 1**). While the voltage was kept at a constant value, the output power of the BFC and BC was constantly declining. This can be ascribed to a gradual deactivation of the enzymes and the concomitant loss in the bioelectrocatalytic current. The power output of the BC is around 50% lower than the power generated by the BFC because part of the power is used to ensure its own functioning.

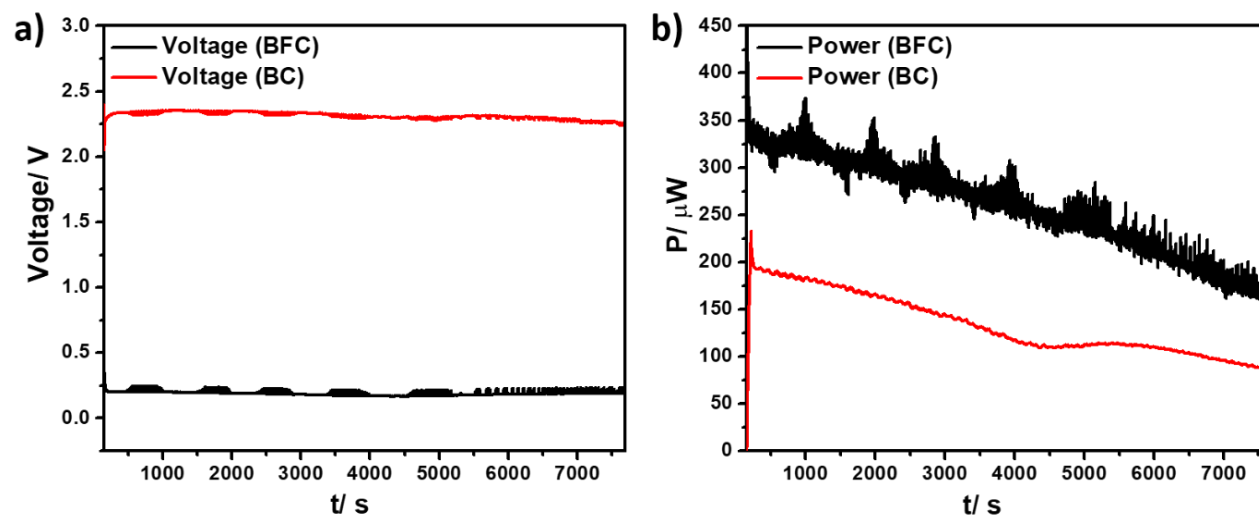


Figure 4. The BFC (black curve) and the BC (red curve) output voltage **a)** and power **b)** curves recorded during a period of 2 h. The BFC was operating at 37.5 °C in oxygen saturated PBS (pH 7.2) supplemented with 50 mM glucose and 20 nM catalase. Oxygen was supplied to the system continuously during the measurement. The corrosion cell was composed of an iron cathode and platinum anode, operating in PBS solution.

The results of the cathodic corrosion protection experiment (**Figure 5**) show that the surface of the sample subjected to 2.3 V for 2 h in PBS buffer remained clean (**Figure 5a**) and free of any corrosion products which can be observed for the control sample that was left to corrode spontaneously in the electrolyte. This clearly demonstrates the possibility to use the very low voltage of such an electrochemical device for successful corrosion protection.

Although most of the current methods for corrosion protection are focusing on the development of new corrosion-resistant materials^{51,52} or organic/inorganic coatings,⁵³ the implementation of bioelectrochemical systems to perform such a demanding task, even for a limited amount of time, is a novel approach that has not been demonstrated earlier. It is worth mentioning that pure iron is the most corrosion prone of all iron-based materials/alloys, which

sets up a very demanding task for the BFC-BC system. Nevertheless, a successful corrosion protection is achieved and maintained while the BFC delivers its maximum power output.

The concept presented in this work can be further extended not only to power electronic devices with relatively low power/voltage requirements and the design of various self-powered electrochemical biosensors, but also to electrochemical systems that will for example synthesize in situ physiologically active molecules.

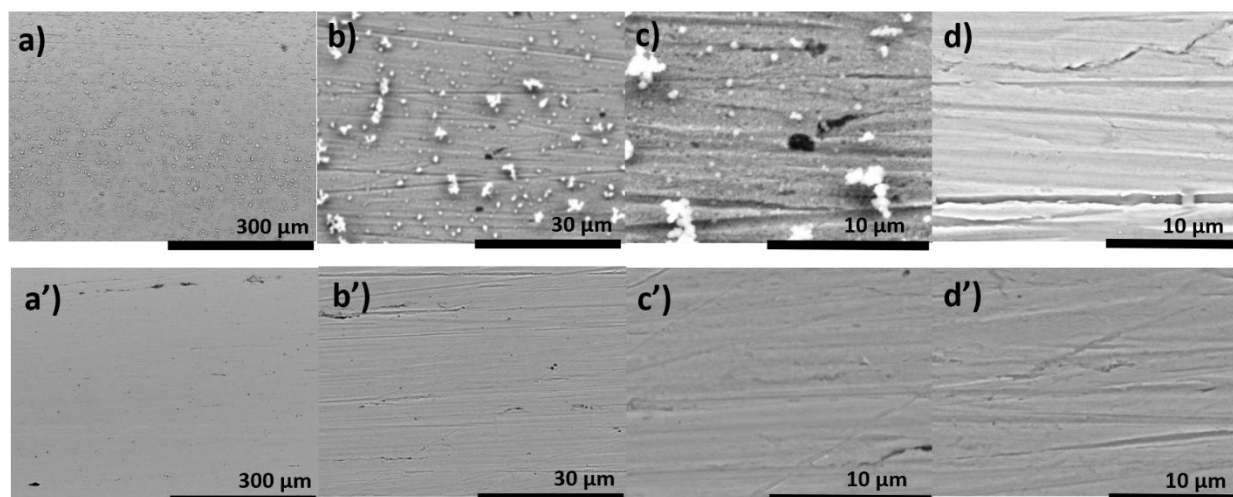


Figure 5. The SEM images of the unprotected control (**a-c**) and the sample that was connected to the BFC delivering a voltage of 2.3 V for 2h (**a'-c'**). For the sake of comparison, the pristine surfaces of both samples are shown in figures **d**) and **d'**), respectively.

Conclusion

In this proof-of-concept study, a new and unconventional way of electrochemical corrosion protection is demonstrated with a model system consisting of a pure iron rod in a chloride rich electrolyte (i.e. PBS buffer). The described strategy is based on using a low-voltage (i.e. 0.3

V)/power (500 μ W) bioelectrochemical device such as an enzymatic glucose/oxygen biofuel cell, modulating its output voltage to higher values *via* a well-adapted electronic circuit (low power boost converter) in order to obtain a final voltage (min. 2.2 V) that fulfills the requirements for successful corrosion protection. A voltage of 2.3 V completely prevents the corrosion process at the surface of the iron rod, as observed by SEM imaging. This clearly validates the present concept as well as the versatility of systems where biofuel cells are efficiently integrated into more complex bioelectronics devices.

ASSOCIATED CONTENT

Supporting information: Corrosion mechanism, Construction of the BFC, Circuit diagram, Potentiodynamic polarization experiment, EDS and SEM analysis, Corrosion evolution study, Electrochemical impedance spectroscopy, Optimization of the CNT-enzymatic hydrogel composite.

The Supporting Information is available free of charge on the ACS Publications website at DOI:

AUTHOR INFORMATION

Corresponding Author

* E-mail: nicolas.mano@crpp.cnrs.fr

* E-mail: kuhn@enscbp.fr

Author Contributions

The manuscript was written through contributions of all authors. All authors have given approval to the final version of the manuscript.

Funding Sources

- Laboratory of Excellence AMADEus (ANR-10-LABX-0042-AMADEUS)
- Agence Nationale de la Recherche” under the program “Initiative for Excellence IdEx Bordeaux” (ANR-10-IDEX-0003–02).

ACKNOWLEDGMENT

This work, realized within the framework of the Laboratory of Excellence AMADEus with the reference ANR-10-LABX-0042-AMADEUS, has benefitted from aid by the state operated “Agence Nationale de la Recherche” under the program “Initiative for Excellence IdEx Bordeaux” holding the reference ANR-10-IDEX-0003–02. The authors thank Isabelle Ly for performing the EDS experiments.

REFERENCES

- (1) Mano, N.; Poulpiquet, De Poulpiquet, A. O₂ Reduction in Enzymatic Biofuel Cells. **2018**.
<https://doi.org/10.1021/acs.chemrev.7b00220>.
- (2) Xiao, X.; Xia, H.; Wu, R.; Bai, L.; Yan, L.; Magner, E.; Cosnier, S.; Lojou, E.; Zhu, Z.; Liu, A. Tackling the Challenges of Enzymatic (Bio) Fuel Cells. *Chem. Rev.* **2019**.
<https://doi.org/10.1021/acs.chemrev.9b00115>.
- (3) Rasmussen, M.; Abdellaoui, S.; Minter, S. D. Enzymatic Biofuel Cells: 30 Years of Critical Advancements. *Biosens. Bioelectron.* **2016**, 76, 91–102.
<https://doi.org/10.1016/j.bios.2015.06.029>.
- (4) Kaiser, P.; Reich, S.; Leykam, D.; Willert-Porada, M.; Greiner, A.; Freitag, R.

- Electrogenic Single-Species Biocomposites as Anodes for Microbial Fuel Cells. *Macromol. Biosci.* **2017**, *17* (7), 1–10. <https://doi.org/10.1002/mabi.201600442>.
- (5) Higgins, S. R.; Lau, C.; Atanassov, P.; Minteer, S. D.; Cooney, M. J. Hybrid Biofuel Cell: Microbial Fuel Cell with an Enzymatic Air-Breathing Cathode. *ACS Catal.* **2011**, *1* (9), 994–997. <https://doi.org/10.1021/cs2003142>.
- (6) Arechederra, R.; Minteer, S. D. Organelle-Based Biofuel Cells: Immobilized Mitochondria on Carbon Paper Electrodes. *Electrochim. Acta* **2008**, *53* (23), 6698–6703. <https://doi.org/10.1016/j.electacta.2008.01.074>.
- (7) Mazurenko, I.; Poulpiquet, A. De; Lojou, E. Recent Developments in High Surface Area Bioelectrodes for Enzymatic Fuel Cells Recent Developments in High Surface Area Bioelectrodes for Enzymatic Fuel Cells. *Curr. Opin. Electrochem.* **2017**, *5* (1), 74–84. <https://doi.org/10.1016/j.coelec.2017.07.001>.
- (8) Pinyou, P.; Blay, V.; Muresan, L. M.; Noguer, T. Enzyme-Modified Electrodes for Biosensors and Biofuel Cells. *Mater. Horiz.* **2019**, *6* (7), 1336–1358. <https://doi.org/10.1039/C9MH00013E>.
- (9) Mano, N. Recent Advances in High Surface Area Electrodes for Bioelectrochemical Applications. *Curr. Opin. Electrochem.* **2019**, No. October, 1–6. <https://doi.org/10.1016/j.coelec.2019.09.003>.
- (10) Liu, Z.; Cho, B.; Ouyang, T.; Feldman, B. Miniature Amperometric Self-Powered Continuous Glucose Sensor with Linear Response. *Anal. Chem.* **2012**, *84* (7), 3403–3409. <https://doi.org/10.1021/ac300217p>.

- (11) Bandodkar, A. J.; Jeerapan, I.; You, J. M.; Nuñez-Flores, R.; Wang, J. Highly Stretchable Fully-Printed CNT-Based Electrochemical Sensors and Biofuel Cells: Combining Intrinsic and Design-Induced Stretchability. *Nano Lett.* **2016**, *16* (1), 721–727. <https://doi.org/10.1021/acs.nanolett.5b04549>.
- (12) Katz, E.; Bückmann, A. F.; Willner, I. Self-Powered Enzyme-Based Biosensors [8]. *J. Am. Chem. Soc.* **2001**, *123* (43), 10752–10753. <https://doi.org/10.1021/ja0167102>.
- (13) Jeerapan, I.; Sempionatto, J. R.; Wang, J. On-Body Bioelectronics: Wearable Biofuel Cells for Bioenergy Harvesting and Self-Powered Biosensing. *Adv. Funct. Mater.* **2019**, *1906243*, 1–18. <https://doi.org/10.1002/adfm.201906243>.
- (14) Gai, P.; Song, R.; Zhu, C.; Ji, Y.; Wang, W.; Zhang, J. R.; Zhu, J. J. Ultrasensitive Self-Powered Cytosensors Based on Exogenous Redox-Free Enzyme Biofuel Cells as Point-of-Care Tools for Early Cancer Diagnosis. *Chem. Commun.* **2015**, *51* (94), 16763–16766. <https://doi.org/10.1039/c5cc07520c>.
- (15) Zhang, L.; Wang, Y.; Ma, C.; Wang, P.; Yan, M. Self-Powered Sensor for Hg²⁺ Detection Based on Hollow-Channel Paper Analytical Devices. *RSC Adv.* **2015**, *5* (31), 24479–24485. <https://doi.org/10.1039/c4ra14154g>.
- (16) Jia, W.; Wang, X.; Imani, S.; Bandodkar, A. J.; Ramírez, J.; Mercier, P. P.; Wang, J. Wearable Textile Biofuel Cells for Powering Electronics. *J. Mater. Chem. A* **2014**, *2* (43), 18184–18189. <https://doi.org/10.1039/c4ta04796f>.
- (17) Katz, E.; MacVittie, K. Implanted Biofuel Cells Operating in Vivo-Methods, Applications and Perspectives-Feature Article. *Energy Environ. Sci.* **2013**, *6* (10), 2791–2803.

<https://doi.org/10.1039/c3ee42126k>.

- (18) Zebda, A.; Cosnier, S.; Alcaraz, J. P.; Holzinger, M.; Le Goff, A.; Gondran, C.; Boucher, F.; Giroud, F.; Gorgy, K.; Lamraoui, H.; Cinquin, P. Single Glucose Biofuel Cells Implanted in Rats Power Electronic Devices. *Sci. Rep.* **2013**, *3*, 1–5. <https://doi.org/10.1038/srep01516>.
- (19) Slaughter, G.; Kulkarni, T. Enzymatic Glucose Biofuel Cell and Its Application. *J. Biochips Tissue Chips* **2015**, *05* (01). <https://doi.org/10.4172/2153-0777.1000110>.
- (20) Xiao, X.; Siepenkoetter, T.; Conghaile, P.; Leech, D.; Magner, E. Nanoporous Gold-Based Biofuel Cells on Contact Lenses. *ACS Appl. Mater. Interfaces* **2018**, *10* (8), 7107–7116. <https://doi.org/10.1021/acsami.7b18708>.
- (21) Zhang, L.; Carucci, C.; Reculosa, S.; Goudeau, B.; Lefrançois, P.; Gounel, S.; Mano, N.; Kuhn, A. Rational Design of Enzyme-Modified Electrodes for Optimized Bioelectrocatalytic Activity. *ChemElectroChem* **2019**, *6* (19), 4980–4984. <https://doi.org/10.1002/celec.201901022>.
- (22) Zebda, A.; Gondran, C.; Le Goff, A.; Holzinger, M.; Cinquin, P.; Cosnier, S. Mediatorless High-Power Glucose Biofuel Cells Based on Compressed Carbon Nanotube-Enzyme Electrodes. *Nat. Commun.* **2011**, *2* (May), 370. <https://doi.org/10.1038/ncomms1365>.
- (23) Xiao, X.; Magner, E. A Biofuel Cell in Non-Aqueous Solution. *Chem. Commun.* **2015**, *51* (70), 13478–13480. <https://doi.org/10.1039/c5cc04888e>.
- (24) MacVittie, K.; Halánek, J.; Halámková, L.; Southcott, M.; Jemison, W. D.; Lobel, R.;

- Katz, E. From “Cyborg” Lobsters to a Pacemaker Powered by Implantable Biofuel Cells. *Energy Environ. Sci.* **2013**, *6* (1), 81–86. <https://doi.org/10.1039/c2ee23209j>.
- (25) Liu, C.; Alwarappan, S.; Chen, Z.; Kong, X.; Li, C. Z. Membraneless Enzymatic Biofuel Cells Based on Graphene Nanosheets. *Biosens. Bioelectron.* **2010**, *25* (7), 1829–1833. <https://doi.org/10.1016/j.bios.2009.12.012>.
- (26) Luz, R. a S.; Pereira, A. R.; Souza, J. C. P. De; Sales, F. C. P. F.; Crespilho, F. N. Enzyme Biofuel Cells : Thermodynamics , Kinetics and Challenges in Applicability. **2014**, 1751–1777. <https://doi.org/10.1002/celc.201402141>.
- (27) Hanashi, T.; Yamazaki, T.; Tsugawa, W.; Ikebukuro, K.; Sode, K. BioRadioTransmitter: A Self-Powered Wireless Glucose-Sensing System. **2011**, *5* (5), 1030–1035.
- (28) Suraniti, E.; Merzeau, P.; Roche, J.; Gounel, S.; Mark, A. G.; Fischer, P.; Mano, N.; Kuhn, A. Uphill Production of Dihydrogen by Enzymatic Oxidation of Glucose without an External Energy Source. *Nat. Commun.* **2018**, *9* (1). <https://doi.org/10.1038/s41467-018-05704-5>.
- (29) Southcott, M.; MacVittie, K.; Halámek, J.; Halámková, L.; Jemison, W. D.; Lobel, R.; Katz, E. A Pacemaker Powered by an Implantable Biofuel Cell Operating under Conditions Mimicking the Human Blood Circulatory System – Battery Not Included. *Phys. Chem. Chem. Phys.* **2013**, *15* (17), 6278. <https://doi.org/10.1039/c3cp50929j>.
- (30) Chen, X.; Yin, L.; Lv, J.; Gross, A. J.; Le, M.; Gutierrez, N. G.; Li, Y.; Jeerapan, I.; Giroud, F.; Berezovska, A.; O'Reilly, R.K. Stretchable and Flexible Buckypaper-Based Lactate Biofuel Cell for Wearable Electronics. *Adv. Funct. Mater.* **2019**, *1905785*, 1–8.

<https://doi.org/10.1002/adfm.201905785>.

- (31) Baingane, A.; Slaughter, G. Self-Powered Electrochemical Lactate Biosensing. *Energies* **2017**, *10* (10), 1–9. <https://doi.org/10.3390/en10101582>.
- (32) Courjean, O.; Gao, F.; Mano, N. Deglycosylation of Glucose Oxidase for Direct and Efficient Glucose Electrooxidation on a Glassy Carbon Electrode. *Angew. Chemie - Int. Ed.* **2009**, *48* (32), 5897–5899. <https://doi.org/10.1002/anie.200902191>.
- (33) Durand, F.; Gounel, S.; Kjaergaard, C. H.; Solomon, E. I.; Mano, N. Bilirubin Oxidase from *Magnaporthe Oryzae*: An Attractive New Enzyme for Biotechnological Applications. *Appl. Microbiol. Biotechnol.* **2012**, *96* (6), 1489–1498. <https://doi.org/10.1007/s00253-012-3926-2>.
- (34) Bartholome, C.; Derré, A.; Roubeau, O.; Zakri, C.; Poulin, P. Electromechanical Properties of Nanotube-PVA Composite Actuator Bimorphs. *Nanotechnology* **2008**, *19* (32). <https://doi.org/10.1088/0957-4484/19/32/325501>.
- (35) Bartholome, C.; Miaudet, P.; Derré, A.; Maugey, M.; Roubeau, O.; Zakri, C.; Poulin, P. Influence of Surface Functionalization on the Thermal and Electrical Properties of Nanotube-PVA Composites. *Compos. Sci. Technol.* **2008**, *68* (12), 2568–2573. <https://doi.org/10.1016/j.compscitech.2008.05.021>.
- (36) Mao, F.; Mano, N.; Heller, A. Long Tethers Binding Redox Centers to Polymer Backbones Enhance Electron Transport in Enzyme “Wiring” Hydrogels. *J. Am. Chem. Soc.* **2003**, *125* (16), 4951–4957. <https://doi.org/10.1021/ja029510e>.

- (37) Cadet, M.; Brilland, X.; Gounel, S.; Louerat, F.; Mano, N. Design of a Highly Efficient O₂ Cathode Based on Bilirubin Oxidase from *Magnaporthe Oryzae*. *ChemPhysChem* **2013**, *14* (10), 2097–2100. <https://doi.org/10.1002/cphc.201300027>.
- (38) A. Ejaz, Q. Xiao, J. Chen, G. Han, Z. L. Effects of Hydrogen on Corrosion Products Formed on Iron in Chloride Solutions. *Trans. E C S Soc. Electrochem.* **2016**, *72* (17), 31–40.
- (39) Wang, Y.; Cheng, G.; Wu, W.; Qiao, Q.; Li, Y.; Li, X. Effect of PH and Chloride on the Micro-Mechanism of Pitting Corrosion for High Strength Pipeline Steel in Aerated NaCl Solutions. *Appl. Surf. Sci.* **2015**, *349*, 746–756. <https://doi.org/10.1016/j.apsusc.2015.05.053>.
- (40) Frankel, G. S. Pitting Corrosion of Metals. *J. Electrochem. Soc.* **1998**, *145* (6), 2186. <https://doi.org/10.1149/1.1838615>.
- (41) Yohai, L.; Schreiner, W.; Valcarce, M. B.; Vázquez, M. Inhibiting Steel Corrosion in Simulated Concrete with Low Phosphate to Chloride Ratios. *J. Electrochem. Soc.* **2016**, *163* (13), C729–C737. <https://doi.org/10.1149/2.0511613jes>.
- (42) Bastidas, D. M.; Criado, M.; Fajardo, S.; La Iglesia, A.; Bastidas, J. M. Corrosion Inhibition Mechanism of Phosphates for Early-Age Reinforced Mortar in the Presence of Chlorides. *Cem. Concr. Compos.* **2015**, *61*, 1–6. <https://doi.org/10.1016/j.cemconcomp.2015.04.009>.
- (43) Ruff, A. Redox Polymers in Bioelectrochemistry: Common Playgrounds and Novel Concepts. *Curr. Opin. Electrochem.* **2017**, *5* (1), 66–73.

<https://doi.org/10.1016/j.coelec.2017.06.007>.

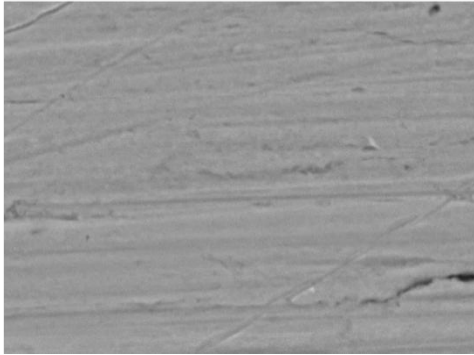
- (44) Heller, A. Electrical Wiring of Redox Enzymes. **1990**, 128–134.
- (45) Heller, A. Miniature Biofuel Cells. *Phys. Chem. Chem. Phys.* **2004**, *6* (2), 209–216.
<https://doi.org/10.1039/B313149A>.
- (46) Barton, S. C.; Gallaway, J.; Atanassov, P. Enzymatic Biofuel Cells for Implantable and Microscale Devices. *Chem. Rev.* **2004**, *104* (10), 4867–4886.
<https://doi.org/10.1021/cr020719k>.
- (47) Katakis, I.; Ye, L.; Heller, A. Electrostatic Control of the Electron-Transfer Enabling Binding of Recombinant Glucose Oxidase and Redox Polyelectrolytes. *J. Am. Chem. Soc.* **1994**, *116* (8), 3617–3618. <https://doi.org/10.1021/ja00087a065>.
- (48) PrévotEAU, A.; Mano, N. Oxygen Reduction on Redox Mediators May Affect Glucose Biosensors Based on “Wired” Enzymes. *Electrochim. Acta* **2012**, *68*, 128–133.
<https://doi.org/10.1016/j.electacta.2012.02.053>.
- (49) Szczesny, J.; Marković, N.; Conzuelo, F.; Zacarias, S.; Pereira, I. A. C.; Lubitz, W.; Plumeré, N.; Schuhmann, W.; Ruff, A. A Gas Breathing Hydrogen/Air Biofuel Cell Comprising a Redox Polymer/Hydrogenase-Based Bioanode. *Nat. Commun.* **2018**, *9* (1), 1–9. <https://doi.org/10.1038/s41467-018-07137-6>.
- (50) Marković, N.; Conzuelo, F.; Szczesny, J.; González García, M. B.; Hernández Santos, D.; Ruff, A.; Schuhmann, W. An Air-Breathing Carbon Cloth-Based Screen-Printed Electrode for Applications in Enzymatic Biofuel Cells. *Electroanalysis* **2019**, *31* (2), 217–221.

<https://doi.org/10.1002/elan.201800462>.

- (51) Farmer, J.; Choi, J. S.; Saw, C.; Haslam, J.; Day, D.; Hailey, P.; Lian, T.; Rebak, R.; Perepezko, J.; Payer, J.; Branagan, D.; Beardsley, B.; D'Amato, A.; Aprigliano, L. Iron-Based Amorphous Metals: High-Performance Corrosion-Resistant Material Development. *Metall. Mater. Trans. A Phys. Metall. Mater. Sci.* **2009**, *40* (6), 1289–1305. <https://doi.org/10.1007/s11661-008-9779-8>.
- (52) Shi, Y.; Yang, B.; Liaw, P. K. Corrosion-Resistant High-Entropy Alloys: A Review. *Metals (Basel)*. **2017**, *7* (2), 1–18. <https://doi.org/10.3390/met7020043>.
- (53) Montemor, M. F. Functional and Smart Coatings for Corrosion Protection: A Review of Recent Advances. *Surf. Coatings Technol.* **2014**, *258*, 17–37. <https://doi.org/10.1016/j.surfcoat.2014.06.031>.

Table of contents (TOC)

Biofuel cell protected surface



Unprotected surface

